ECS Journal of Solid State Science and Technology, **6** (4) N32-N37 (2017)
2162-8769/2017/6(4)/N32/6/$37.00 © The Electrochemical Society

Nanofiber-Structured TiO_2 Nanocrystals as a Scattering Layer in Dye-Sensitized Solar Cells

F. Navarro-Pardo,[a] D. Benetti,[a] J. Benavides,[b] H. G. Zhao,[a,z] S. G. Cloutier,[b] V. M. Castano,[c] A. Vomiero,[d,z] and F. Rosei[a,*,z]

[a]*Centre for Energy, Materials and Telecommunications, Institut National de la Recherche Scientifique, Varennes (QC) J3X1S2, Canada*
[b]*Département de Génie Électrique, École de Technologie Supérieure, QC H3C 1K3 Montréal, Canada*
[c]*Centre of Applied Physics and Advanced Technology, National Autonomous University of Mexico, Santiago de Querétaro, C.P. 76230 Juriquilla, México*
[d]*Division of Engineering Sciences and Mathematics, Luleå University of Technology, 97187 Luleå, Sweden*

We developed a scattering layer composed of TiO_2 nanocrystals assembled into a densely packed three-dimensional network of nanofibers to localize light within a photoanode used in dye sensitized solar cells (DSSCs). The electro-netting approach was applied to obtain polyamide 6 nanofibers with bi-modal diameter distribution, followed by solvothermal synthesis for the coating of TiO_2 nanocrystals on the polymer template. The resulting nanofiber-structured scattering layer (NFSL) is composed of TiO_2 nanofibers (200–300 nm in diameter) supporting an ultrathin nanofiber network (diameters within 10–50 nm) and exhibits strong light scattering in the visible range (400 to 700 nm). This NFSL was applied on top of a transparent active TiO_2 layer (TL) forming the photoanode in DSSCs. The performance of the bi-layered photoanode was compared to its analogue, fabricated with commercial scattering layers containing different sizes of nanoparticles. The DSSCs assembled with the NFSL showed an 18% enhancement in power conversion efficiency (PCE) compared to that of DSSCs whose photoanode contained only a TL. This enhancement factor was improved up to 31% when the bi-layered structure was post-treated with $TiCl_4$. The PCE improvement was mainly associated with the light harvesting efficiency within the photoanode because of scattering from the NFSL and increased dye adsorption due to the addition of this top layer. These conclusions were inferred from diffuse reflectance behavior, dye loading measurements, external quantum efficiency and electrochemical properties. Our work demonstrates a promising approach without the requirement of time consuming and complicated procedures for the fabrication of a densely packed 3D nanofiber network scattering layer for diverse energy conversion devices and photocatalytic applications.
 [DOI: 10.1149/2.0181704jss]

Manuscript submitted November 28, 2016; revised manuscript received January 24, 2017. Published February 15, 2017.

The development of one-dimensional (1D) nanomaterials with controllable structure and properties is being widely studied, particularly geared at applications in electronics, photonics, biomedical technologies and energy[1,2–5] A large number of advanced techniques can be employed to obtain these 1D structures in the form of nanorods, nanotubes, nanowires, nanoribbons or nanobelts and nanofibers.[2] Among these techniques, electrospinning stands out as a simple, low cost and scalable approach for producing nanofiber networks. Features such as fiber density and multi-layered structure make them ideal candidates for various applications, such as filtration, sensors and composites.[3] The feasibility of shaping the structure and morphology of the fibers and the suitability of polymers to make composites with metal oxide semiconductors represents a promising approach for their exploitation in excitonic solar cells, such as dye-sensitized solar cells (DSSCs), quantum dot-sensitized solar cells and perovskite-sensitized solar cells.[4,6–11] DSSCs are attractive due to their relatively low manufacturing cost, comparable high photoconversion efficiencies (PCE), wider range of colors and light weight compared to conventional silicon solar cells.[12] A typical DSSC consists of a semiconducting oxide active layer where dye molecules are adsorbed, a redox couple electrolyte and a counter-electrode.[1,12] The PCE can be improved by adopting different strategies, including enhancing the light-harvesting of the dye,[13] tailoring the composition of the electrolyte,[14,15] or engineering the device to increase charge collection and reduce recombination.[4,6–8] Within the latter, modification of the photoanode relies on approaches to tailor its morphology and/or its composition.[16–18] This element of a DSSC device is typically composed of TiO_2, ZnO or SnO_2 nanoparticles (NPs) with average diameter sizes of ∼20 nm.[1,6–8] Even if sensitized by the most efficient dyes with the highest extinction coefficients, a photoanode made only of small (∼20 nm) nanoparticles is unable to guarantee full light absorption. The addition of a scattering overlayer is a common approach to localize the incident light within the photoanode and enhance the light absorption by increasing the optical path length and the time spent by light within the photoanode; thus, this scattering overlayer can enhance the final photocurrent density of the device.[16,17] Large spherical NPs (sizes larger than 100 nm)[16,17,19–21] or 1D nanostructures[22–26] are used as top layers in the photoanode due to their ability to scatter light.[22,23] One of the drawbacks of the generally used spherical and 1D nanostructures is that dye adsorption is low, due to their reduced surface area.[17,21] Several strategies have been developed to improve dye adsorption in the scattering layers, such as the growth of hierarchical structures[24,27] and other combinatorial methods to increase porosity.[21,23] In particular, 1D nanostructures obtained by electrospinning polymer-based sol-gel solutions suffer from a high volume of macropores among the TiO_2 fibers; this morphology limits the harvesting of solar light.[22] A high density of 1D structures can be achieved by grinding fibers into nanorods and/or mixing them with NPs.[22,25] Nevertheless, in comparison with spherical NPs, 1D nanostructures have shown promising results as scattering layers due to efficient light reflection and high electron diffusion coefficients.[22] To further improve PCE the photoanodes are post-treated with $TiCl_4$.[22–26] The post-treatment reduces the pore volume of 1D nanostructures while improving their inter-connectivity and enhancing electron diffusion.[28] Therefore, most of the above-mentioned approaches involve long preparation times for the hydrothermal reaction (24 h or longer) and additional multiple steps to make pastes and/or the use of toxic chemicals for inducing porosity or improving electron transfer. To obtain a scattering layer based on fibers that possess high surface area with a safe and simple approach is still very challenging.

Herein we report the optimization of a process for obtaining a three-dimensional (3D) highly packed network of TiO_2 nanocrystals comprising 1D structures with bi-modal diameter. This cost-effective approach involves a process termed "electro-netting"[3,29–31] followed by the solvothermal method. Electro-netting of polyamide 6 (PA6) allows the macropores within the main large diameter fibers to be filled with nanofibers of smaller diameter assembled into a spider-like network. These bi-modal diameter nanofiber films (BDNFs) served as a sacrificial template for the deposition of TiO_2 nanocrystals and

*Electrochemical Society Member.
[z]E-mail: zhaoh@emt.inrs.ca; alberto.vomiero@ltu.se; rosei@emt.inrs.ca

were applied as a nanofiber scattering layer (NFSL) on top of a transparent layer (TL) of TiO_2 NPs. The resulting bi-layered photoanode was compared to analogous photoanodes prepared with commercial scattering layers and assembled in DSSCs. Our results showed that DSSCs fabricated with the NFSL exhibit an increased PCE originating from the enhanced light trapping ability within the photoanode, which was inferred by means of diffuse reflectance, external quantum efficiency, dye loading measurements and electrochemical characterization. These results indicate that the bi-modal structured nanofiber can be used as a high efficiency scattering layer in DSSC, with potential use in other energy conversion devices which require large and uniform areas with increased porosity.

The DSSCs assembled with NFSL showed an 18% enhancement in PCE compared to that of DSSCs whose photoanode was composed only of a TiO_2 transparent active layer. This enhancement increased to 31% when the bi-layered photoanode was post-treated with $TiCl_4$. The PCE improvement is mainly associated with the light harvesting efficiency within the photoanode because of the scattering from the NFSL and increased dye adsorption due to the addition of the top layer. This work demonstrates a promising approach for the fabrication of a densely packed 3D network of bi-modal diameter nanofibers comprising TiO_2 nanocrystals capable of trapping light within the photoanode, without the requirement of time consuming and complicated procedures, which this type of 1D-structured scattering layers typically involve.

Methods

Electro-netting of PA6.—Bi-modal diameter nanofiber films were obtained in an electrospinning unit (Spraybase, Profector Life Sciences) at 20 kV using a 26G gauge needle and a 15 cm distance between needle and grounded collector. PA6 pellets (Sigma Aldrich) were dissolved in formic acid (FA, Sigma Aldrich). Polymer solution parameters such as concentration (17, 20, 23 wt%) and solution stirring time (4, 24 h) were tuned to obtain the BDNFs with small diameter fibers covering the whole area of the main fibers' macropores. Electrospinning flow rate and deposition time were modified to optimize the conditions for achieving the desired thickness of the BDNF structured films.

TiO_2 coating of BDNFs.—A dispersion of TiO_2 NP_S was prepared by sonicating for one hour 2 wt% TiO_2 NPs (considering a 80% weight loss of organics after removing the organics in the TiO_2 18 NR-T, Dyesol paste) in ethanol (Sigma Aldrich). BDNFs were electrospun onto FTO glasses (sheet resistance 10 Ωsq^{-1}) for one hour, then the sample was placed in a 20 mL Teflon-lined cup and filled with 15 mL of the TiO_2 dispersion, placed inside a stainless-steel autoclave vessel and heated to the desired temperature (140, 160 or 180°C) which was then held for different residence times (2, 5 and 14 h). Three sets of samples were prepared for each condition. Afterwards the autoclave was cooled to room temperature and the samples were immersed in 10 mL of ethanol for 15 min and then dried at ambient conditions for 10 mins.

Photoanode and solar cell fabrication.—DSSCs were fabricated according to standard procedures.[6–8] All photoanodes consist of an active transparent layer produced from TiO_2 anatase NPs with average size of 20 nm (18 NR-T, Dyesol) tape casted on FTO glass substrates. The thickness of the photoanode was controlled by using a scotch tape (50 μm) or two tapes stacked on top of each other (100 μm) as the spacers to cast the TiO_2 paste and the corresponding samples were labeled as single transparent layer (STL) or double transparent layer (DTL) photoanodes. The films were dried for 15 min at ambient temperature and then for 6 min at 120°C. Film thickness was measured using a Dektak profilometer and it was found that the STL and the DTL were ∼6 or ∼12 μm thick, respectively. The commercial pastes were tape casted on the TL photoanodes, repeating the same tape-casting procedure and employing only one scotch tape.

Bi-layered photoanodes were fabricated consisting of DTL and scattering layers made with commercial pastes: (i) wide diameter TiO_2 NPs with size ranging from 150–250 nm (WER2-O, Dyesol), samples identified as DTL + WSL and (ii) mixture of TiO_2 NPs with active anatase NPs (20 nm) and larger anatase scatter particles with diameters up to 450 nm (18 NR-AO, Dyesol), samples labeled as DTL + MSL. After drying, all photoanodes were sintered in ambient atmosphere according to the following steps: 200°C for 15 min, 400°C for 15 min and 500°C for 30 min. All the sintered DTL photoanodes were treated by UV/Ozone for 20 min in an Ossila UV Ozone cleaning system. For the photoanodes containing the NFSL, the STL or DTL were first tape-casted and sintered as described above and then the nanofibers were electrospun for one hour onto any of these TLs. These photoanodes were labeled as xTL + NFSL, being x = S or D according to the thickness of the active layer. The bi-layer structure was dried at 70°C for 15 min before conducting the solvothermal reaction at 180°C. Subsequently, the polymer was removed and the NFSL was sintered by using the same heating conditions as reported previously (this second sintering process was used for all the fabricated photoanodes). All photoanodes were sensitized for 24 hours in a 0.5 mM solution of Ru-based complex molecular N719 dye (Dyesol) in ethanol (Sigma Aldrich). Subsequently, the photoanodes were washed with ethanol to remove any unbound dye molecules. DSSCs were prepared by using a 25 μm thick Surlyn film (Solaronix) between the photoanode and a counter-electrode composed of a 10 nm Pt/Pd (80/20 wt%) sputter-coated layer onto FTO glass (sheet resistance 8 Ωsq^{-1}). The cells were closed and filled using a I/I_3^- redox couple electrolyte (Solaronix HI-30).

Characterization.—The morphology of the samples was characterized using a field-emission scanning electron microscope (FE-SEM) JEOL JSM7401F. The current–voltage characteristics of the fabricated cells were measured using an Agilent Keysight 5900 under simulated sunlight from an ABET2000 solar simulator at AM 1.5G (100 $mW \cdot cm^{-2}$) calibrated using a reference silicon cell and mechanical filters. The relative volumetric dye concentration in the photoanodes was determined by desorbing the dye into 0.1 M aqueous NaOH solution of known volume for 20 h and measuring the solution absorbance by UV-Visible (Vis) spectrometer using a Varian Cary 5000 UV−Vis−near infrared (NIR) spectrophotometer. The absorbance was taken at 500 nm in wavelength and the data was normalized to the photoanode volume. The external quantum efficiency was measured in an IQE 200 Oriel apparatus using a 250 W quartz tungsten halogen lamp, monochromator, an optical chopper, a lock-in amplifier, and a calibrated silicon photodetector. Electrochemical impedance spectroscopy (EIS) was carried out in the dark using a SOLARTRON 1260A impedance/gain-phase analyzer, while applying a 10 mV AC bias from 100 mHz to 300 kHz. The applied bias during measurements in the dark was varied between 0 and 100 mV above the open-circuit voltage of the solar cell under illumination. All the samples were measured inside a Faraday cage.

Results and Discussion

An SEM cross-section image of the bi-layer photoanode architecture is displayed in the Figure 1. The NFSL (thickness ∼2.5 μm) was obtained by electro-netting of PA6. This polymer has the ability to form conventional electrospun fibers, acting as a support for interlinked ultrathin nanofibers.[3,29–31] The main fibers have diameters of hundreds of nanometers, while the diameters of the ultrathin nanofibers are in the range of 10–50 nm (Figure 2a). The density of the ultrathin nanofibers can be controlled mainly by varying polymer concentration, changing solvents or tuning the applied voltage.[29–31] As seen in Figure S1, there is a lower threshold of solution concentration for the formation of the small diameter fibers: the ultrathin nanofibers are formed at PA6/FA solution concentration not lower than 20 wt%. Further increase of the concentration to 23 wt% leads to the full coverage of the ultrathin interconnected nanofibers within the main polymer fiber framework. Their density was also dependent on

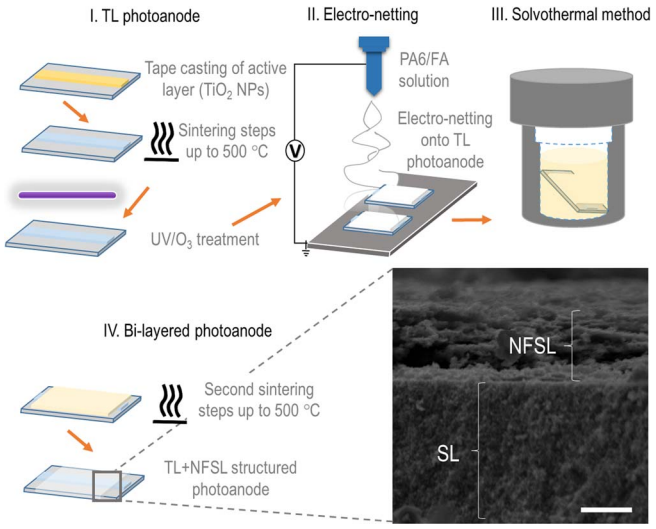

Figure 1. Scheme showing the bi-layered photoanode preparation steps and STL + NFSL cross section. SEM scale bar equals 2 μm.

the polymer solution stirring time, the solution stirred for 24 h showed a higher density of ultrathin nanofibers compared to the ones obtained at the same solution concentration. The optimal conditions of solution concentration for obtaining bi-modal diameter fibers are similar to the ones used in previous works.[30,31] Additionally, we also found that by fixing the polymer concentration solution and electrospinning parameters these ultrathin nanofibers are developed as the electro-netting deposition time is increased. As displayed in Figure S2, increasing the nanofiber deposition time from 40 s to 90 s results in a higher density of both main nanofibers and ultrathin nanofibers. After 1 h of deposition a highly dense 3D network composed of bi-modal diameter nanofibers was developed. Nanofiber deposition time was also studied to obtain the film thicknesses; the data is reported in Table S1. An optimum flow rate of 0.06 mL/h and deposition time of one hour was chosen. Higher flow rates produced drops of the solution on the film during nanofiber deposition, while lower flow rates yielded very thin films; preliminary tests showed that annealing the bi-modal diameter nanofiber films at 200°C reduced the film to half its initial thickness, which was further reduced after solvothermal treatment due to shrinkage of nanofibers. Solvothermal synthesis was performed at different temperatures and residence times, as seen in Figures 2b–2h: temperatures of 140, 160 and 180°C were chosen. Treatment times from 2 to 14 h were applied for 140 and 160°C. Prolonged synthesis (longer than 5 h) yielded films with agglomerated NPs, mainly concentrated on the large NF's macropores, burying both main and ultrathin NFs completely (Figure 2e and 2h). Solvothermal conditions applied for 30 minutes at 180°C provided a better TiO_2 NP coating onto the bi-modal diameter nanofiber films (Figure 2b) and this condition was used to obtain a NFSL over a transparent active layer of TiO_2 NPs (bi-layered photoanode), shown in Figure 1. After polymer removal, the diameter of the main nanofibers ranges from 200 to 300 nm. A top view of the densely packed network of TiO_2 nanocrystals disposed into the ultrathin fibers within the main polymer fiber framework can be found in Figure S3. Higher magnification images of our NFSL fabricated under the optimal conditions is displayed in Figure S4a. The main fiber morphology persists after polymer removal, after which a porous structure was developed, incorporating TiO_2 nanocrystals assembled into a highly packed three-dimensional (3D) architecture. The ultrathin fibers filled up the macropores of the main fibers, making them look like the composites commonly obtained when mixing NPs and ground fibers (nanorods).[22] As opposed to the flat films obtained after solvothermal treatment where agglomerated TiO_2 NPs were deposited atop the ultrathin network of nanofibers (Figure S4b). In addition to designing a time-saving and easy procedure, the materials obtained in this work offer the advantage of having pre-fabricated BDNFs and being solvothermally-treated at any time before attaching them to an active layer of previously UV/Ozone treated TiO_2 NPs. This procedure cannot be employed with the typical nanofibers obtained from titanium precursors and binder polymers, since these films crack easily and detach from substrates even before polymer removal.

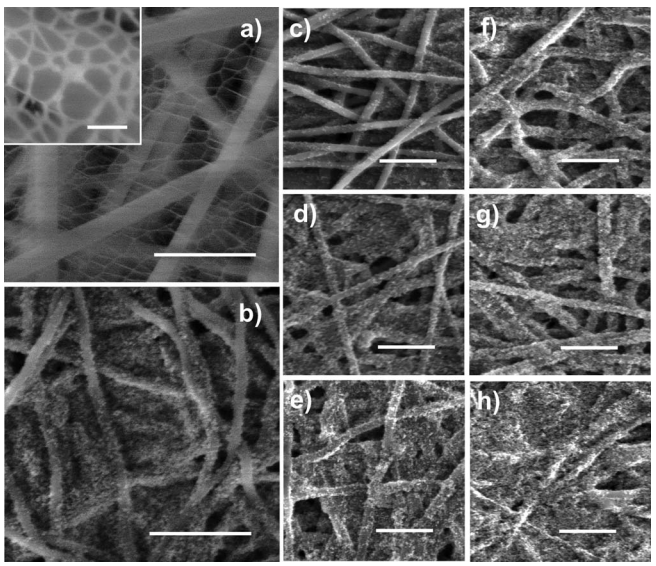

Figure 2. SEM images of (a) PA6 BDNF, inset showing the ultrathin nanofibers and (b) Optimal condition of TiO_2 NP coating on PA6 BDNF after solvothermal treatment at 180°C for 30 min. Coating of nanofibers by solvothermal method at different conditions. (c), (d), and (e) were obtained at 140°C for 2, 5 and 14 h, respectively. (f), (g), and (h) were treated at 160°C for 2, 5 and 14 h, respectively. Scale bar equals 1 μm and inset scale bar equals 100 nm.

The performance of the NFSL has been compared to that of commercial scattering layers, which are typically used to enhance light harvesting. Accordingly, we prepared bi-layer structured photoanodes by tape casting a layer of commercial scattering pastes including NPs with different dimensions, i.e. NPs with diameter size similar to the diameter size of the main diameter nanofibers (WSL) and another containing a mixture of active TiO_2 NPs and larger diameter NPs acting as light-trapping centers within the photoanode (MSL). The morphology of the fabricated bi-layered photoanodes is shown in Figure 3. Kim et al[27] studied the effect of different thicknesses and photoanode morphologies; they have shown that for the active layer composed of NPs, the optimum thickness is ~12 μm, similar to the one used herein. They also found that the optimal thickness for efficient light harvesting changes according to the morphology of the scattering medium.

Nanofiber films cannot exceed a certain threshold thickness when electrospun directly on conducting substrates. Thicker films undergo shrinkage leading to detachment from the substrate and the formation of cracks is predominant when the composite film is sintered to remove organic precursors.[10,32,33] Several procedures have been developed to favor adhesion to substrates or to the TiO_2 nanoparticle films, including the use of a pre-deposited TiO_2 thin adhesive layer[34] and/or solvent post-treatment[35] and hot pressing,[36] making the process rather time-consuming and more complicated. Due to the aforementioned reasons, thin nanofiber films are preferable (<3 μm), whereas spherical NPs used as scattering layers with thicknesses within 5–10 μm have been found to provide improved performance in DSSCs.[10,27]

We therefore tested DSSCs composed of NFSL with thicknesses ~2.5 μm and commercial scattering layers with thicknesses ~5.5 μm, which are the typical thicknesses obtained by tape-casting or screen-printing one layer of commercial paste.[27] Figure 3 shows the top view of the active layer and the bi-layered photoanodes, displaying the different morphologies achieved for the scattering layers. Additionally, the bottom insets display the photoanodes after dye-sensitization.

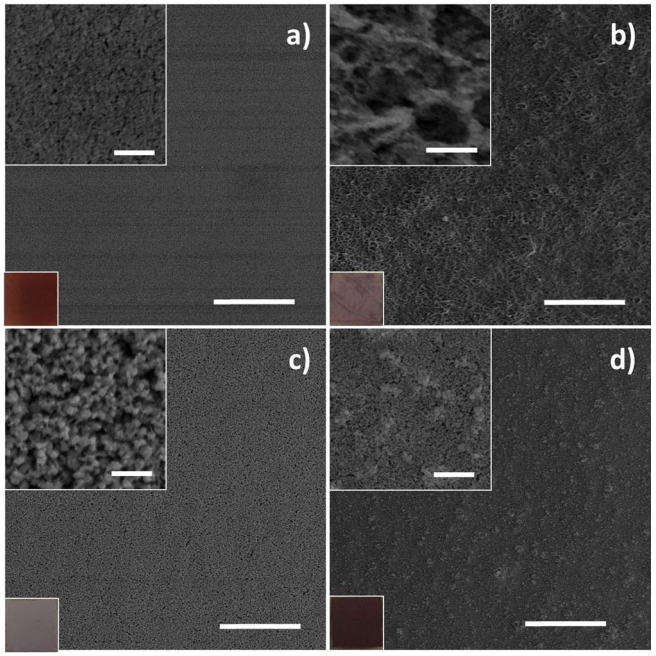

Figure 3. SEM and digital images of the photoanodes. (a) DTL, (b) NFSL (c) WSL and (d) MSL. SEM scale bar: 10 μm in low magnification images and 1 μm in top insets. The lower insets represent the photoanode after sensitization, square dimension: 25 × 25 mm^2.

There is no obvious color in the WSL due to the reduced specific surface of this film, compared to mesoporous films composed of small (20 nm) NPs. In contrast, the photoanode prepared with the MSL shows a dark pink color indicating a higher amount of dye loading in this top layer, due to the adsorbed dye molecules by the small size TiO_2 NPs. Dye loading measurements by UV-Vis spectroscopy clarified this observation, as seen in Figure S5a; these results suggest that the dye adsorption capacity in the WSL is negligible and the dye is mainly adsorbed in the active layer whereas the photoanode with the NFSL adsorbed a slightly higher amount of dye (as displayed in Figure 5b).

Figure 4a shows the current density vs. voltage plots (*J-V*). The functional parameters are summarized in Table I. After inclusion of the NFSL, we observed an increase of ∼6% in both J_{sc} and V_{oc} for the DSSC made with a single transparent layer (STL), leading to an enhancement of 21% in the PCE. A thicker active transparent layer (DTL) favors the adsorption of dye molecules, which is reflected in the further enhancement of the J_{sc}. In contrast, the V_{oc} is reduced; this observation has been previously explained in terms of the increased charge recombination and mass transport limitations in the thicker films and the increase in the series resistances due to redox species and electron migration through a longer path-length to complete the circuit.[19,37] The data also shows the improved light harvesting when adding scattering layers. Specifically, the advantage of including a NFSL is clearly seen by the enhancement in the J_{sc}, leading to a PCE improvement of 18% compared to photoanodes containing only active TiO_2 NPs. This performance is higher than that of the DSSC assembled with the WSL. A decrease in both J_{sc} and V_{oc} in the photoanode made with the MSL can be related to the larger amount of small size TiO_2 NPs when compared to the larger size ones, which are limited to poor light harvesting and higher recombination. Sun et al.[24] recently reported a bi-layered photoanode composed of TiO_2 nanotubes acting as a scattering layer (featuring similar dimensions to the structures developed in our work). Their bi-layered photoanode was pre and post-treated with $TiCl_4$ and used in DSSCs, resulting in a PCE enhancement of only 5%. Further increase of their scattering layer thickness resulted in a PCE improvement of 12%. As a reference, they also compared their scattering layer to commercial grade spherical NPs (diameter ∼500 nm) for which the PCE enhancement factor was ∼5%.[24]

The EQE is directly related to the amount of dye adsorbed mainly in the active layers and the scattering behavior of the top layers. As such, the addition of larger particles of size comparable to the wavelength of incident light promotes light-trapping within the photoanode, especially in the 650–800 nm region, where the N719 sensitizer has a low absorption efficiency (<20%).[37,38] As seen in Figure 4b, the EQE is enhanced in the whole spectral region when adding the scattering layers. The main nanofiber framework in the NFSL consists of larger nanofibers with an average diameter size of ∼200 nm, which can contribute to back-scatter the light that passes through the active layer, as seen by the enhanced spectra of this sample compared to the DTL photoanode. The DTL + NFSL show the highest EQE at low wavelengths (450–550 nm) when compared to photoanodes with commercial scattering layers. This occurrence can be attributed to both the scattering effect of the NFSL and the higher increase of the dye loading in this sample. In contrast, the commercial NP-based scattering layers show a broader spectra at wavelengths longer than 570 nm, which can be attributed to both the high packing of the NPs

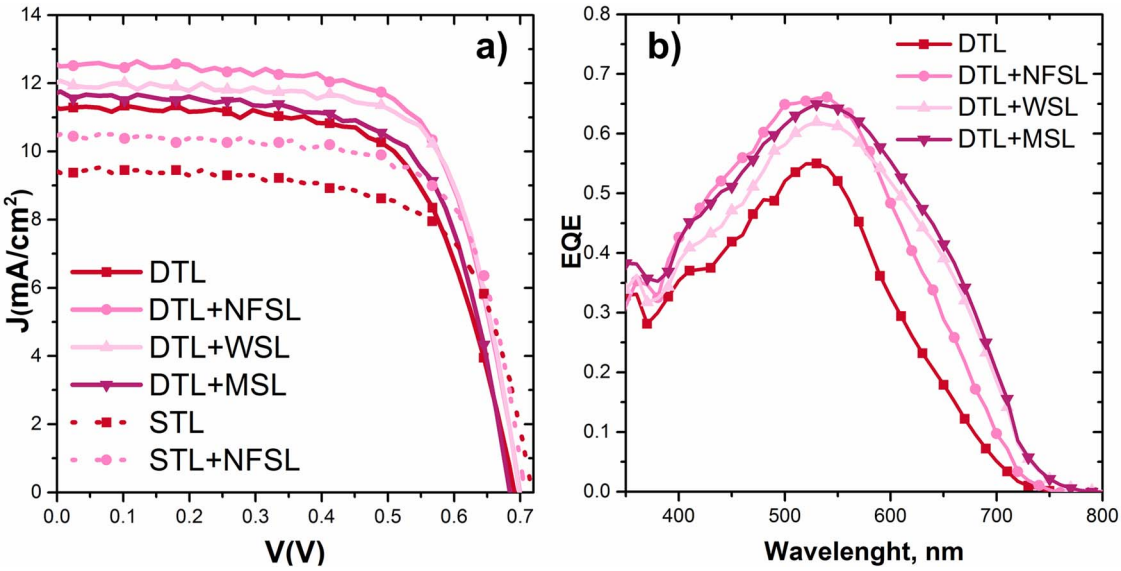

Figure 4. (a) J-V curves of DSSCs with different photoanodes. (b) EQE spectra of DSSCs with different structured photoanodes.

Table I. Functional properties of DSSCs under 1 sun irradiation (AM1.5G, 100 mW cm^{-2}).

Sample	Thickness, μm	J_{sc}, mA · cm^{-2}	V_{oc}, V	FF	PCE (%)
STL	5.9 ± 1.0	8.9 ± 0.3	0.71 ± 0.02	0.68 ± 0.01	4.2 ± 0.2
STL + NFSL	7.5 ± 0.9	9.4 ± 0.3	0.75 ± 0.01	0.71 ± 0.01	5.1 ± 0.2
DTL	12.2 ± 0.8	11.3 ± 0.4	0.70 ± 0.01	0.68 ± 0.01	5.1 ± 0.1
DTL + NFSL	14.4 ± 1.0	12.6 ± 0.8	0.70 ± 0.02	0.69 ± 0.01	6.0 ± 0.1
DTL + WSL	18.7 ± 1.0	12.0 ± 0.1	0.70 ± 0.01	0.70 ± 0.01	5.9 ± 0.2
DTL + MSL	18.2 ± 0.8	11.7 ± 0.9	0.68 ± 0.04	0.67 ± 0.01	5.4 ± 0.1

in the WSL and the NPs with large sizes in the MSL. Diffuse reflectance measurements of the bi-layered photoanode confirmed the scattering ability of these samples (Figure 5). The photoanode composed of WSL achieved higher reflectance under both frontal and rear illumination. As seen in Figure 5b when testing the samples under rear illumination (closer conditions to the *J-V* test under simulated light), the back reflection of the WSL when light travels through the DTL is only ∼3% higher than the rest of the scattering layers. Therefore, all the bi-layered photoanodes showed comparable scattering efficiencies and this higher ability to reflect light compensates the slightly lower dye loading in the bi-layered photoanode.

Electron transport properties of the DSSCs with the best performances were investigated using EIS. We focused on the recombination resistance (R_{rec}) and chemical capacitance (C_{μ}), shown in Figure 6. Higher values of R_{rec} are desired as this is an indicator of a reduced charge recombination.[39,40] However, as seen in Figure 6a, at low voltage bias, R_{rec} is slightly lower in the DTL + NFSL. At low bias conditions (up to 300 mV), R_{rec} takes into account the recombination phenomena between the FTO, TiO_2 layer and electrolyte.[41] In these conditions, the main contribution to R_{rec} comes from the uncovered FTO substrate at the bottom of the TiO_2 film (the back layer).[40,42] As also visible in SEM images, the NFSL presents a larger porosity than the WSL. This can lead to a higher exposed area of the back layer and consequently to an increased charge transfer between the FTO, the TiO_2 layer and the electrolyte. A similar behavior has been observed in similar structures in which a higher recombination was attributed to an increased number of surface trap states, which act as centers for recombination of electrons within the electrolyte.[36] The chemical capacitance is very similar for all the samples, indicating that there is no shift in the conduction band of the TiO_2.[40] An efficient way to reduce the charge recombination at the TiO_2 interfaces (which in turn improves the efficiency DSSCs), is to introduce a thin blocking layer. Previous studies used a $TiCl_4$ pre- and post-treatment[22–24] and/or the introduction of carbon nanomaterials[7,43,44] to improve charge transport. Regardless of the slight increase in recombination when adding the NFSL on top of the active layer, the scattering behavior developed by the main nanofibers and increased dye loading due to the intricate 3D network in the NFSL provides a good compromise for enhancing the performance of DSSCs. As mentioned previously, most research on DSSCs relies on the $TiCl_4$ treatments, which we further conducted in the DTL + NFSL. These treatments are normally done before tape casting the TiO_2 pastes and after sintering the photoanodes. However, to avoid longer preparation times, we applied the post-treatment immediately after the solvothermal synthesis. The *J-V* test and functional properties highlighted in Figure S6 shows that this additional treatment leads to an increase of 31% in the PCE for the DSSCs with the NFSL, compared to the cells assembled only with the active layer.

Conclusions and Perspectives

We tailored electro-netting and solvothermal treatment conditions to obtain bi-dimensional diameter nanofibers, which can be fabricated directly on top of active layers of TiO_2 NPs over large and uniform areas, to be used as photoanodes in DSSCs. According to the performance measured for devices assembled with this nanofiber scattering layer, a PCE enhancement of 18% was achieved in these bi-layered photoanodes (DTL + NFSL), compared to the active transparent photoanode (DTL). This thin layer (∼2.5 μm) based on two dimensional nanofibers features both light-trapping ability within the photoanode due to the main fibers and increased dye loading due to the densely-packed and the porous network comprising ultrathin nanofibers. Our results are comparable to the scattering layers obtained with commercial pastes, which rely on the incorporation of higher amounts of NPs (∼5.5 μm thick layers). A further increase in the PCE (31%)

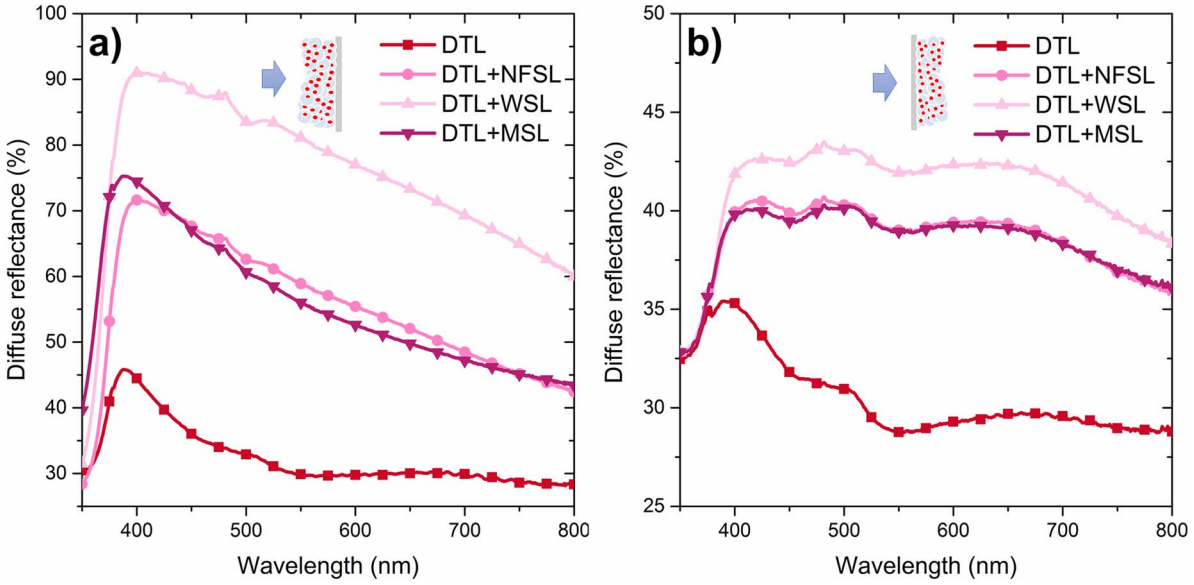

Figure 5. Diffuse reflectance spectra measured under (a) front and (b) rear illumination.

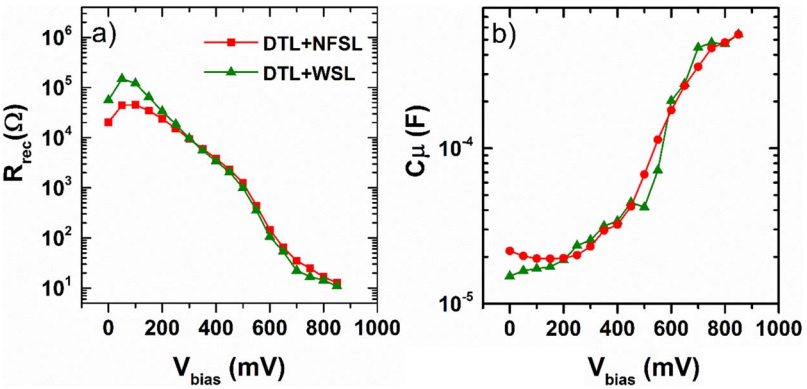

Figure 6. EIS analysis of DSSCs with different scattering layers. (a) Recombination resistance and (b) chemical capacitance from EIS measurements in dark.

was achieved when the DTL + NFSL was post-treated with $TiCl_4$. These results demonstrate that the time-efficient and facile processing proposed in this work allows the fabrication of nanostructured films consisting of an intricate 3D network with features that improve low-cost light-harvesting performances, relevant for DSSCs and other solar energy devices which comprise photoanodes such as photoelectrochemical cells for water splitting, quantum dot-sensitized solar cells and solid state perovskite-sensitized solar cells.

Acknowledgments

F. R. acknowledges NSERC for funding through the Discovery Grants program and for an EWR Steacie Memorial Fellowship for funding and partial salary support. F. R. is grateful to the Alexander von Humboldt Foundation for a F. W. Bessel Award. A. V. acknowledges Kempe Foundation and LTU Lab fund program for funding. F. N. P. is grateful for a postdoctoral fellowship from Fonds de recherche du Québec – Nature et technologies (FRQNT) and CONACYT (grant 236094).

References

1. I. Concina and A. Vomiero, *Small*, **11**, 1744 (2015).
2. X. Lu, C. Wang, and Y. Wei, *Small*, **5**, 2349 (2009).
3. X. Wang, B. Ding, G. Sun, M. Wang, and J. Yu, *Prog. Mater. Sci.*, **58**, 1173 (2013).
4. F. Navarro-Pardo, D. Benetti, H. Zhao, V. Castaño, A. Vomiero, and F. Rosei, *J. Power Sources*, **335**, 138 (2016).
5. F. Navarro-Pardo, L. Jin, R. Adhikari, X. Tong, D. Benetti, K. Basu, S. Vanka, H. G. Zhao, Z. T. Mi, S. H. Sun, V. M. Castano, A. Vomiero, and F. Rosei, *Mater. Chem. Front.*, **1**, 65 (2017).
6. K. T. Dembele, G. S. Selopal, C. Soldano, R. Nechache, J. C. Rimada, I. Concina, G. Sberveglieri, F. Rosei, and A. Vomiero, *J. Phys. Chem. C*, **117**, 14510 (2013).
7. D. Benetti, K. T. Dembele, J. Benavides, H. Zhao, S. Cloutier, I. Concina, A. Vomiero, and F. Rosei, *J. Mater. Chem. C*, **4**, 3555 (2016).
8. K. Basu, D. Benetti, H. Zhao, L. Jin, F. Vetrone, A. Vomiero, and F. Rosei, *Sci. Rep.*, **6**, 23312 (2016).
9. B. O'Regan and M. Grätzel, *Nature*, **353**, 737 (1991).
10. S. Dharani, H. K. Mulmudi, N. Yantara, P. T. T. Trang, N. G. Park, M. Graetzel, S. Mhaisalkar, N. Mathews, and P. P. Boix, *Nanoscale*, **6**, 1675 (2014).
11. K. Dembele, R. Nechache, L. Nikolova, A. Vomiero, C. Santato, S. Licoccia, and F. Rosei, *J. Power Sources*, **233**, 93 (2013).
12. M. Grätzel, *Nature*, **414**, 338 (2001).
13. B. E. Hardin, H. J. Snaith, and M. D. McGehee, *Nat. Photonics*, **6**, 162 (2012).
14. M. Wang, N. Chamberland, L. Breau, J.-E. Moser, R. Humphry-Baker, B. Marsan, S. M. Zakeeruddin, and M. Grätzel, *Nat. Chem.*, **2**, 385 (2010).
15. A. Yella, H.-W. Lee, H. N. Tsao, C. Yi, A. K. Chandiran, M. K. Nazeeruddin, E. W.-G. Diau, C.-Y. Yeh, S. M. Zakeeruddin, and M. Grätzel, *Science*, **334**, 629 (2011).
16. K.-J. Hwang, J.-Y. Park, S. Jin, S. O. Kang, and D. W. Cho, *New J. Chem.*, **38**, 6161 (2014).
17. H. J. Koo, Y. J. Kim, Y. H. Lee, W. I. Lee, K. Kim, and N. G. Park, *Adv. Mater.*, **20**, 195 (2008).
18. L. Yang and W. W. F. Leung, *Adv. Mater.*, **23**, 4559 (2011).
19. W.-G. Yang, F.-R. Wan, Q.-W. Chen, J.-J. Li, and D.-S. Xu, *J. Mater. Chem.*, **20**, 2870 (2010).
20. H.-J. Koo, J. Park, B. Yoo, K. Yoo, K. Kim, and N.-G. Park, *Inorg. Chim. Acta*, **361**, 677 (2008).
21. S. H. Han, S. Lee, H. Shin, and H. Suk Jung, *Adv. Energy Mater.*, **1**, 546 (2011).
22. P. Joshi, L. Zhang, D. Davoux, Z. Zhu, D. Galipeau, H. Fong, and Q. Qiao, *Energy Environ. Sci.*, **3**, 1507 (2010).
23. S. H. Hwang, C. Kim, H. Song, S. Son, and J. Jang, *ACS Appl. Mater. Interfaces*, **4**, 5287 (2012).
24. K. C. Sun, M. B. Qadir, and S. H. Jeong, *RSC Adv.*, **4**, 23223 (2014).
25. M. Jalali, R. S. Moakhar, A. Kushwaha, G. K. L. Goh, N. Riahi-Noori, and S. K. Sadrnezhaad, *Electrochim. Acta*, **169**, 395 (2015).
26. Y.-L. Chen, Y.-H. Chang, J.-L. Huang, I. Chen, and C. Kuo, *J. Phys. Chem. C*, **116**, 3857 (2012).
27. D. H. Kim, W. M. Seong, I. J. Park, E.-S. Yoo, S. S. Shin, J. S. Kim, H. S. Jung, S. Lee, and K. S. Hong, *Nanoscale*, **5**, 11725 (2013).
28. B. H. Lee, M. Y. Song, S.-Y. Jang, S. M. Jo, S.-Y. Kwak, and D. Y. Kim, *J. Phys. Chem. C*, **113**, 21453 (2009).
29. S.-Y. Tsou, H.-S. Lin, and C. Wang, *Polymer*, **52**, 3127 (2011).
30. R. Nirmala, H. R. Panth, C. Yi, K. T. Nam, S.-J. Park, H. Y. Kim, and R. Navamathavan, *Macromol. Res.*, **18**, 759 (2010).
31. R. Nirmala, K. T. Nam, S.-J. Park, Y.-S. Shin, R. Navamathavan, and H. Y. Kim, *Appl. Surf. Sci.*, **256**, 6318 (2010).
32. S. Lee, J. Ha, J. Choi, T. Song, J. W. Lee, and U. Paik, *ACS Appl. Mater. Interfaces*, **5**, 11525 (2013).
33. K. Fujihara, A. Kumar, R. Jose, S. Ramakrishna, and S. Uchida, *Nanotechnology*, **18**, 365709 (2007).
34. R. Zhu, C.-Y. Jiang, X.-Z. Liu, B. Liu, A. Kumar, and S. Ramakrishna, *Appl. Phys. Lett.*, **93**, 013102 (2008).
35. S. Chuangchote, T. Sagawa, and S. Yoshikawa, *Appl. Phys. Lett.*, **93**, 33310 (2008).
36. K. Mukherjee, T.-H. Teng, R. Jose, and S. Ramakrishna, *Appl. Phys. Lett.*, **95**, 012101 (2009).
37. T. Deepak, G. Anjusree, S. Thomas, T. Arun, S. V. Nair, and A. S. Nair, *RSC Adv.*, **4**, 17615 (2014).
38. L. I. Halaoui, N. M. Abrams, and T. E. Mallouk, *J. Phys. Chem. B*, **109**, 6334 (2005).
39. F. Fabregat-Santiago, J. Bisquert, E. Palomares, L. Otero, D. Kuang, S. M. Zakeeruddin, and M. Grätzel, *J. Phys. Chem. C*, **111**, 6550 (2007).
40. F. Fabregat-Santiago, J. Bisquert, G. Garcia-Belmonte, G. Boschloo, and A. Hagfeldt, *Sol. Energy Mater. Sol. Cells*, **87**, 117 (2005).
41. J. Bisquert, I. Mora-Sero, and F. Fabregat-Santiago, *ChemElectroChem*, **1**, 289 (2014).
42. L. Peter, N. Duffy, R. Wang, and K. Wijayantha, *J. Electroanal. Chem.*, **524**, 127 (2002).
43. L. Yang and W. W. F. Leung, *Adv. Mater.*, **25**, 1792 (2013).
44. T. J. Macdonald, D. D. Tune, M. R. Dewi, C. T. Gibson, J. G. Shapter, and T. Nann, *ChemSusChem*, **8**, 3396 (2015).